

# Compact closed-loop resonator filters with wide spurious free band and extended common-mode noise suppression

ISSN 1751-8725  
 Received on 1st July 2019  
 Revised 19th November 2019  
 Accepted on 26th February 2020  
 E-First on 1st June 2020  
 doi: 10.1049/iet-map.2019.0581  
 www.ietdl.org

Arcesio Arbelaez<sup>1</sup> ✉, Jose-Luis Olvera<sup>2</sup>, Alonso Corona<sup>2</sup>, Carlos Saavedra<sup>1</sup>

<sup>1</sup>Department of Electrical and Computer Engineering, Queen's University, Kingston, Ontario, Canada

<sup>2</sup>Department of Electronics, National Institute of Astrophysics, Optics and Electronics (INAOE), Puebla, Puebla, Mexico

✉ E-mail: arcesioarbelaez@gmail.com

**Abstract:** A theoretical analysis is presented for miniaturised filters with an extended stopband and extended common-mode (CM) rejection, using loaded closed-loop resonators. A numerical method is presented to solve the equations extracted from the ideal transmission line model. Selection of critical resonator parameters to minimise filter area while simultaneously maximising the differential-mode (DM) stopband or the CM noise suppression is explored. The trade-off between size, stopband and CM rejection is presented and used to design three filters at 1 GHz, which are designed to verify the proposed concept. First, a differential second-order filter with an extended DM stopband ( $S_{21d} < -20$  dB) up to  $6.8f_c$  and extended CM noise suppression ( $S_{21c} < -20$  dB) up to  $6.42f_c$  is realised to show the parameter trade-offs. Then optimal resonators are used to develop a compact singled-ended filter ( $0.011\lambda_g^2$ ) with an extended stopband ( $S_{21} < -30$  dB) up to  $8.2f_c$  and the smallest size. Lastly, a second order filter with an optimal extended CM rejection ( $S_{21c} < -20$  dB) up to  $6.64f_c$  is presented. Measured results are presented. All three filters stand out compared to other works by exhibiting the smallest footprint relative to the operating frequency.

## 1 Introduction

Balanced filters offer important benefits for communications systems such as reduced noise sensitivity, high common-mode (CM) attenuation and reduced levels of radiation [1, 2]. As with all filters, design parameters for balanced filters include not only bandwidth, stopband rejection, insertion loss and return loss but also CM rejection. Many of these metrics can be directly improved through the choice of the resonator. A quarter wavelength resonator can be used to extend the stopband of a passband filter, due to the lowest spurious frequency being three times the resonant frequency. Compared to a half-wave resonator, where the lowest spurious frequency is only twice the resonant frequency [3]. Another common method to extend a filter's stopband is through the use of stepped impedance resonators (SIR) or closed-loop resonators. Here the spurious frequency position can be controlled through the resonators impedance and length ratios of the connected transmission lines [4, 5]. The inclusion of transmission zeros where the spurious frequency occurs is another common method for stopband extension [6–10].

CM noise suppression is a key metric in differential filter design. The CM response of a balanced bandpass filter should appear as a bandpass filter, while the CM passband frequency must be separate from the differential-mode (DM) passband. The CM resonant frequency can be partially controlled to get the best performance, depending on the type of resonator used. Under CM operation, a quarter wavelength resonator is transformed into a half-wave resonator, due to a virtual open circuit appearing on the differential resonator's line of symmetry. Thus, the CM resonant frequency will always be higher than the DM resonant frequency. Both SIR [4] and closed-loop resonators [11] have proven to be good options for common-noise suppression, without the need for an additional stopband structure [12]. In [13], CM parallel resonances are used to improve the CM response of the filter. A combination of SIR resonators and interdigital capacitors is used in [12] to get improved DM and CM responses.

While minimising the physical size of a filter has always been an important goal in their design, size reduction is paramount in differential filters, particularly at long wavelengths. For a compact filter design the main task, of course, is to miniaturise its

constituent resonators. Several techniques exist to miniaturise a resonator. In [5], for instance, a shorted stub is used to reduce the size of a closed-loop resonator by 93.7%. An inter-digital capacitor is implemented in [14] to reduce the size of a coupled-line filter. Another option is shown in [15], where a multi-mode resonator is used to reduce the number of resonators. Interdigital capacitors are also used to decrease the size as is presented in [14]. In [16], folded SIRs are used to get a compact size filter in comparison with a conventional SIR based filter. In [6] a single-ended SIR filter is reported having a stop-band is 12 times higher than the central frequency ( $f_s = 12f_c$ ) using substrate integrated coaxial line technology and relies on 3 distinct resonators.

In this paper, theoretical analysis and design method are presented for closed-loop resonators with a shorted stub that minimises resonator size and yields either optimal CM noise suppression or extended DM stopband. A transmission line model for a closed-loop resonator and shorted stub is used to obtain the fundamental resonant equation under DM and CM operations. The resulting equations are numerically solved to find the resonance conditions. Using the equations, the resonator can be designed for the minimal area, best-case extended DM stopband and best-case CM noise suppression. Practical constraints are accounted for in the analysis to check the feasibility of the proposed resonators. To validate the design method, two differential filters and a single-ended filter are synthesised, fabricated and measured. The differential filters exhibit very wide DM and CM stopbands that compare well relative to published works and, notably, they occupy a record-low area relative to their operating wavelength as a result of the resonator geometry optimisation.

## 2 Closed-loop resonator using open and short-circuited stubs

A filter's design parameters are usually selected to give either a compact size, an improved CM noise suppression or an extended DM stopband. The standard process focuses on designing resonators with one of these parameters in mind. The main question to answer is how to choose the optimal design parameters to receive either an extended DM stopband, extended CM noise

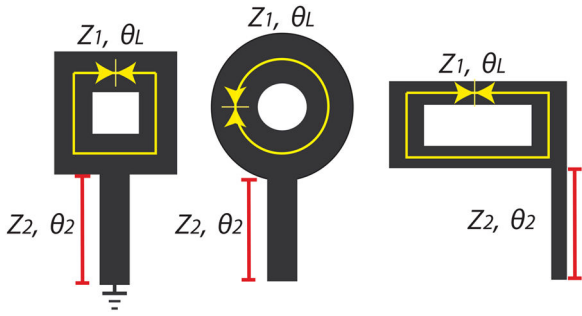


Fig. 1 Microstrip closed-loop resonators with shorted or opened stubs

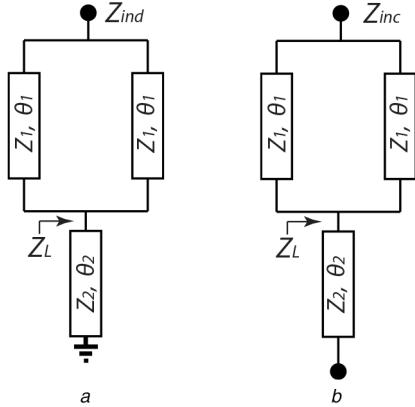


Fig. 2 Closed-loop resonator with a shorted/opened stub model (a) DM equivalent, (b) CM equivalent

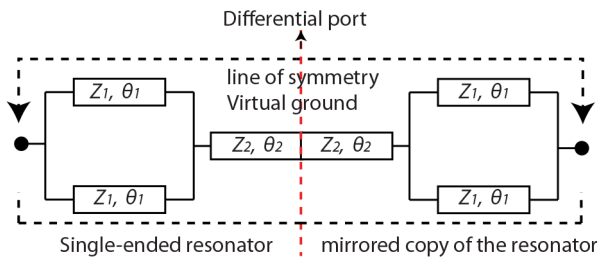


Fig. 3 Microstrip closed-loop differential resonators

suppression while maintaining a compact-sized resonator. To keep the balance between these three parameters an accurate design process is required. The previous methods mentioned above only focus on how to improve a filters performance by taking into account practical considerations and intrinsic advantages of the resonator, but not how to originally design the optimal resonator for the required performance.

### 2.1 Analytic framework

The physical size of a closed-loop resonator can be reduced and its performance improved by using short-circuited stubs [17] or open-circuited stubs [18]. Fig. 1 shows different shapes of a closed-loop resonator with an attached stub. The closed-loop is a transmission line with characteristic impedance  $Z_1$  and electrical length  $\theta_L$ , while the stub is a transmission line with characteristic impedance  $Z_2$  and electrical length  $\theta_2$ , ending in a short or open circuit. An arbitrary shape can be implemented for the resonator as the loop is closed and has a uniform impedance.

Fig. 2a shows the model of the closed-loop resonator with a shorted stub. This structure is the DM equivalent circuit for a differential resonator. Fig. 2b shows the equivalent model of a closed-loop resonator with an open stub, which is also the CM equivalent circuit of a differential resonator. Here, the electrical length of the closed-loop is  $\theta_L = 2\theta_1$ , with the same impedance  $Z_1$ .

As the DM and CM equivalent circuits have the same model as the single-ended resonators, it is possible to use the same design analysis for differential and single-ended resonators. Thus, first a

single-ended resonator can be designed with the desired response. Then a differential resonator can be obtained by adding a mirrored copy of the single-ended resonator along the axis of symmetry as shown in Fig. 3.

The resonance condition of the equivalent differential model seen in Fig. 2a, is obtained when the denominator of the equivalent impedance  $Z_{ind}$  is zero. The input impedance of the resonator is given by (1)

$$Z_{ind} = \frac{1 + Z_L Y_{22}}{Z_L (Y_{11} Y_{22} - Y_{12} Y_{21}) + Y_{22}}, \quad (1)$$

where

$$Y_{11} = Y_{22} = -\frac{2j}{Z_1} \cot \theta_1, \quad (2)$$

$$Y_{12} = Y_{21} = \frac{2j}{Z_1} \csc \theta_1, \quad (3)$$

and

$$Z_L = jZ_2 \tan \theta_2. \quad (4)$$

Thus, the resonance condition is given by (5), where  $R_z = Z_1/Z_2$  is the impedance ratio of and  $N = \theta_2/\theta_1$  is the length ratio of the loop and stub respectively.

$$\tan \theta_1 \tan(N\theta_1) = \frac{R_z}{2}, \quad (5)$$

The resonance condition for the CM equivalent seen in Fig. 2b is similarly obtained by first calculating the input impedance  $Z_{inc}$ . Here the load impedance  $Z_L$  is given by (6)

$$Z_L = -jZ_2 \cot \theta_2, \quad (6)$$

and the resonance condition is given by (7).

$$\tan \theta_1 \cot(N\theta_1) = \frac{R_z}{2}. \quad (7)$$

### 2.2 Discussion

Equations (5) and (7) require a numerical solution. The control parameters,  $R_z$  and  $N$ , were previously introduced and the properties of the closed-loop resonator can be drastically modified by choosing the appropriate values for these parameters. The physical length of the lines can be calculated once a value for  $\theta_1$  is found from (5) at the desired centre frequency.

A flowchart of the design procedure is shown in Fig. 4. Here, the first step is to define the values of the control parameters  $R_z$  and  $N$ . Then an angles array is defined ( $\theta_1$ ), sweeping the electrical length of the closed loop resonator from zero to its maximum,  $\pi/2$ . Using (5) and (7) we define two equations:  $x = \tan(\theta_1)\tan(N\theta_1)$  and  $v = R_z/2$ , which represent the left- and right-hand side of the resonance equation given in (5). Two values are obtained when solving  $x = v$ , representing the resonant ( $f_o$ ) and first spurious frequency ( $f_s$ ), which provides information on the stopband extension. Then this electrical length is used in (7) to yield the CM resonant frequency ( $f_{oc}$ ).

Once the analysis method is automated it is possible to make a sweep of the control parameters to check the effects of its variation on the DM and CM responses of the resonator. For clarity, the centre frequency is called  $f_o$ , the spurious frequency is called  $f_s$  and the CM resonant frequency is  $f_{oc}$  henceforth.

Fig. 5 shows the variation of the spurious frequency with respect to the control parameters  $R_z$  and  $N$ . Here  $f_s$  can be moved to higher frequencies by choosing small values for  $R_z$  or by choosing a larger value for  $N$ . In practical cases, it is difficult to

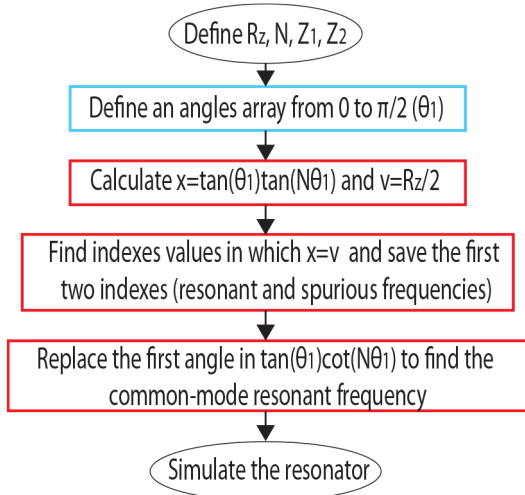


Fig. 4 Flowchart of the analysis method used

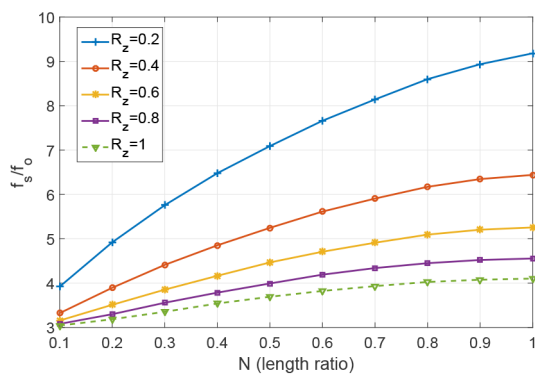


Fig. 5 Variation of the spurious frequency with  $R_z$  and  $N$

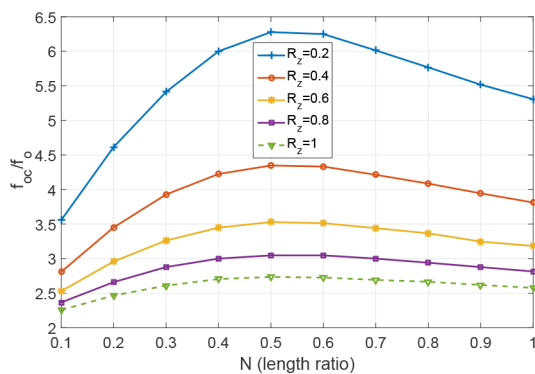


Fig. 6 Variation of the CM resonant frequency with  $R_z$  and  $N$

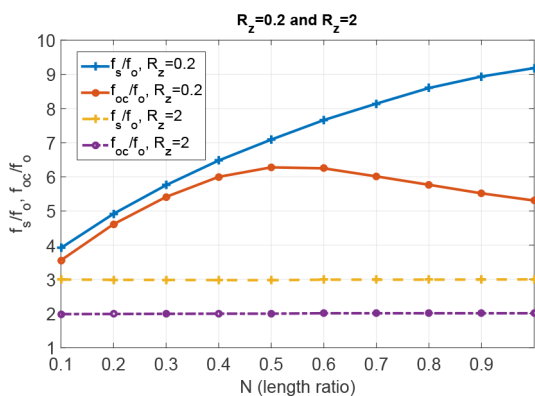


Fig. 7 Special case with  $R_z = 2$

fabricate resonators with a larger  $R_z$ , due to the implementation of the high impedance lines.

Fig. 6 shows the variation of the CM resonant frequency with respect to the control parameters. Unlike the first case, the CM resonant frequency cannot be improved for values of  $N > 0.5$ . Thus, the best-case CM response will be always limited to the case where the length of the high impedance line is half the length of the closed-loop line ( $\theta_2 = \theta_1$ ).

Values of  $R_z < 0.2$  are not considered, as resonators with these impedance ratios are not easily realised in practice. Additionally, values of  $R_z > 1$  are not considered because in that range the resonator starts to behave like a  $\lambda/4$  uniform impedance resonator [19] as shown in Fig. 7 which depicts what occurs when  $R_z = 2$ , for example. Similarly, values of  $N > 1$  are not considered because as the length of the high-impedance line increases, it dominates the main resonator, leading to a standard  $\lambda/4$  resonator.

Fig. 8 shows the variation of the normalised length of the resonator with respect to the control parameters. The normalised length is calculated by adding the size of both lines, then this result is divided by the guided wavelength, always equalling  $2\pi$ . It is clear that the smallest resonator will be the one with the smallest value of  $R_z$  and the highest value of  $N$ , which also is the condition for the best spurious frequency case.

Using Figs. 5 and 6, resonators with the optimal CM response and the spurious response can be obtained. Based on the plots, the best-case spurious frequency is when  $R_z = 0.2$  and  $N = 1$  giving  $f_s/f_o = 9.2$  and  $f_{oc}/f_o = 5.3$ . The best-case for the CM resonant frequency occurs when  $R_z = 0.2$  and  $N = 0.5$ , giving  $f_{oc}/f_o = 6.3$  and  $f_s/f_o = 7.1$ . The ideal responses of the designed resonators are shown in Fig. 9. It is important to mention that there will be minor variations in the response due to the numerical approach (finite decimals) used to solve the resonance equations.

### 3 Practical considerations

The previous section showed the best closed-loop resonator cases predicted by the theory. The aspect ratio of a transmission line is the relation between the width and the length of the line. When the aspect ratio is high, there can be instances where the best-case theoretical resonators cannot be physically implemented because the loop will overlap on itself at the centre. Since the impedance values for  $R_z$  depend on the properties of the substrate and the operating frequency, the designer should select a substrate with a higher dielectric constant or smaller height, both of which will lower the transmission line aspect ratio.

A square closed-loop resonator is implemented in this paper to simplify the analysis. Fig. 10 shows the physical dimensions of the closed-loop resonator with a stub. The dimensions of the inner square for the closed loop resonator is  $d_1 \times d_1$ . There are some practical limitations introduced by the minimum length of  $d_1$ . The smallest square that can be fabricated will be constrained by the resolution of the fabrication process. Equation (8) can be used to calculate the dimensions of the inner square,  $d_1$ , which must be greater than the minimal resolution attainable by the chosen fabrication method. Equation (9) yields  $d_1$  for the case of circular closed-loop resonators

$$d_1 = \frac{L_1}{4} - W_1, \quad (\text{square loop}) \quad (8)$$

$$d_1 = \frac{L_1}{\pi} - W_1. \quad (\text{circular loop}) \quad (9)$$

A second condition is defined by (10)

$$W_2 < \frac{L_2}{4} + W_1 \quad (10)$$

which indicates when the width of the high impedance line is wider than a single side of the square closed-loop. The effects of the impedance transition are not modelled by the ideal transmission

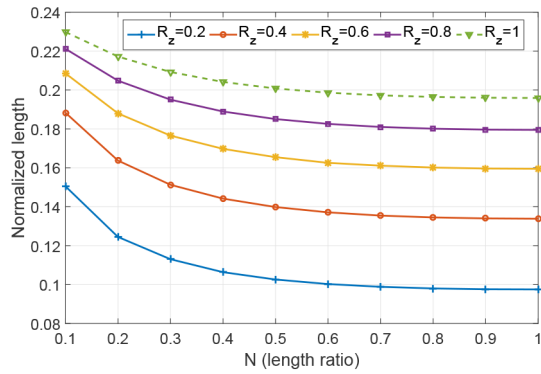


Fig. 8 Variation of the resonator's size with  $R_z$  and  $N$

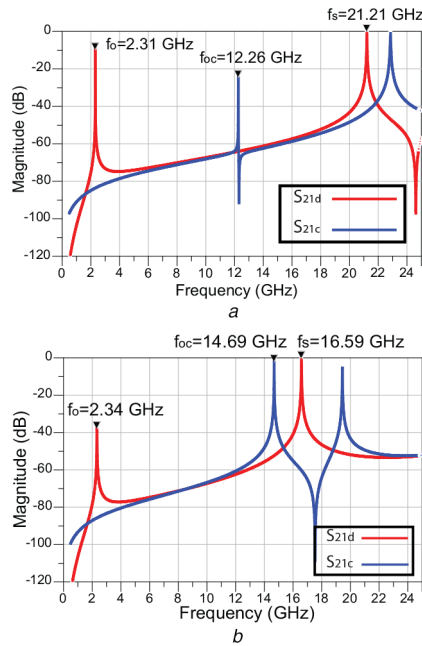


Fig. 9 Closed-loop resonators  
(a) Smallest and best-case spurious response, (b) Best-case CM resonant frequency

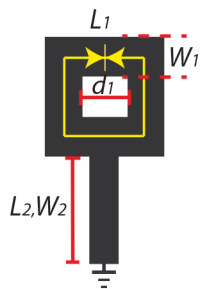


Fig. 10 Closed-loop resonator

line model and there are additional parasitics associated with the physical implementation of the resonator arising from transmission line corners, vias, fabrication tolerance and others. These parasitics can be captured by adding lumped components to the model but it turns out that the proposed transmission line model is robust enough by itself to yield close predictions of filter performance as will be shown in Section 4.

#### 4 Proposed filters

The proposed method is used to develop three filters with compact size, extended stopband, and extended CM noise suppression. The minimum value of  $d_1$  was set to 1 mm. All filters were designed with a centre frequency of  $f_c = 1$  GHz.

#### 4.1 Filter A

The first filter is shown in Fig. 11 and it corresponds to a proof of concept prototype with  $R_z = 0.25$  and  $N = 0.4$  provides a trade-off between the spurious frequency and the CM resonant frequency. The filter is a second-order Butterworth filter with  $FBW = 12\%$ . The low-pass prototype values are:  $g_0 = 1$ ,  $g_1 = 1.4142$  and  $g_2 = 1.4142$ . The required external quality factor is  $Q_e = 9.5$  and the required mutual coupling factor is  $M_{12} = 0.1$ . These frequencies can be extrapolated from Figs. 5 and 6 obtaining  $f_s \approx 6.5f_c$  and  $f_{oc} \approx 6f_c$ . The physical dimensions, the DM spurious frequency and the CM resonant frequency are in Table 1.

#### 4.2 Filter B: designing for minimum size and best-case spurious response

The proposed design method can certainly be used to design single-ended filters. Fig. 12 shows a prototype single-ended filter with the smallest size and the best-case spurious frequency response. From Figs. 5 and 8 it is clear that the smallest resonator will be the one with  $N = 1$  and a small value of  $R_z$ . The best case is when  $R_z = 0.2$ ; however, in order to simplify the filter fabrication a value of  $R_z = 0.25$  is selected. The filter is a third-order Butterworth filter with a  $FBW = 10\%$ . The low-pass prototype values are:  $g_0 = 1$ ,  $g_1 = 1$ ,  $g_2 = 2$  and  $g_3 = 1$ . The required external quality factor is  $Q_e = 10$  and the required mutual coupling factors are  $M_{12} = M_{23} = 0.071$ . In this case, the  $f_s$  will be between  $6f_c$  and  $9f_c$ . Table 2 shows a summary of the resonator properties.

#### 4.3 Filter C: designing for best-case CM noise suppression

Fig. 13 shows the prototype filter with the most extended CM noise suppression band. The design parameters can be extracted from Fig. 6, in this case  $N$  must be 1 and a small value of  $R_z$  is desired. The filter is a third-order Butterworth filter with a  $FBW = 12\%$ . The low-pass prototype values are:  $g_0 = 1$ ,  $g_1 = 1.4142$  and  $g_2 = 1.4142$ . The required external quality factor is  $Q_e = 9.5$  and the required mutual coupling factor is  $M_{12} = 0.1$ . An impedance ratio of  $R_z = 0.3$  is selected, which indicates that  $f_{oc}$  will be larger than  $4.5f_c$ . Table 3 shows a summary of the resonator properties.

### 5 Measured results

The fabricated filters are shown in Fig. 14. These were fabricated on a Rogers 4003C substrate ( $\epsilon_r = 3.55$  and  $h = 0.81$  mm), with a 0.5-oz copper cladding using an LDK ProtoMat circuit plotter. The balanced filters were measured using a four-port VNA. The connector used in all the ports was a solderless amphenol SF1521-60107 port.

The fractional bandwidth (FBW) for all cases is similar to the target values of 10–12%. Filter B (responses in Fig. 15) exhibits a higher variation of the FBW due to the high dependence on the mutual coupling factor with the length of the high impedance line due to the quality of the vias and the fact that the impedance of the high-impedance lines experience a larger variation from fabrication tolerances because they are narrow. The insertion loss of the filters at the central frequency is close to the typically reported insertion loss in microstrip technology [11].

All the filters exhibit an extended stopband. Filters A (DM and CM responses in Fig. 16) and C were not originally designed to have an extended DM stopband. While the filter B, has the most extended DM stopband in microstrip technology without additional structures reported in the literature with attenuation better than -30 dB up to  $8.2f_c$ .

There is the possibility to include additional structures to extend even more the stopband, but it is not considered in this work. It is possible to make a differential filter based on the single-ended filter B by using the technique described in Fig. 3 and it is expected that such a filter would have many of the same characteristics of the single-ended version.

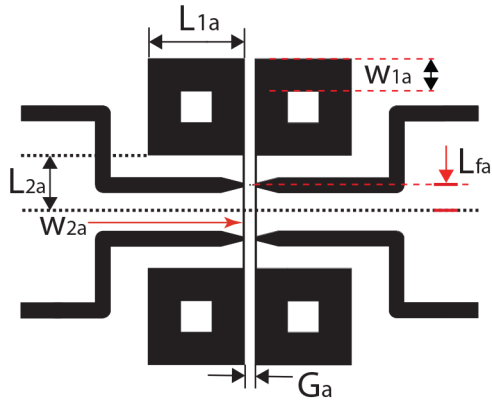


**Fig. 11** Proof of concept prototype filter  $R_z = 0.25$  and  $N = 0.4$ .  $G_a = 1.17$  mm,  $L_{fa} = 3.07$  mm

**Table 1** Dimensions and resonant frequencies of resonator A

Parameter	Value	Model	Full-wave sim.
$L_{1a}$ , mm	11.11	n/a	n/a
$W_{1a}$ , mm	3.76	n/a	n/a
$L_{2a}$ , mm	6.5	n/a	n/a
$W_{2a}$ , mm	0.23	n/a	n/a
$d_{1a}$ , mm	3.59	n/a	n/a
$f_{oa}$ , GHz	n/a	0.99	0.9125
$f_{sa}$ , GHz	n/a	5.95	6.425
$f_{oca}$ , GHz	n/a	5.39	5.275

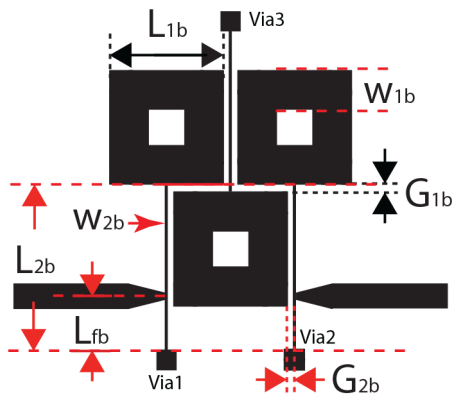


**Fig. 12** Smallest and best-case spurious case prototype filter  $R_z = 0.3$  and  $N = 1$ .  $G_{1b} = 0.485$  mm,  $G_{2b} = 0.365$  mm,  $L_{fb} = 3.684$

Filter C (DM and CM responses in Fig. 17) exhibits an extended CM noise suppression band which is better than  $-20$  dB up to  $6.61f_c$ . The CM passband attenuation is lower than  $-20$  dB. Thus, the proposed resonator appears very promising for the design of high order balanced passband filters with increased CM noise suppression performance. All of the proposed filters exhibit compact size without the need for additional methods to decrease the size.

Table 4 shows a comparison between Filters A and C and related differential filters. Only microstrip filters have been included in order to make a fair comparison. Table 5 compares Filter B with state-of-the-art single-ended loop filters. In both tables, the filters designed using the proposed methodology occupy the smallest area. They also exhibit competitive DM and CM stopbands. The stopband of Filter B is  $8.2f_c$ , which is noticeably better than [5, 14, 16], whose stopbands are  $4f_c$ ,  $5.7f_c$  and  $3f_c$ , respectively. While the filter in [6] has a wider stopband of  $12f_c$  that filter uses 3 different resonator topologies, whereas Filter B uses only 1 type of resonator.

**Table 2** Dimensions and resonant frequencies of resonator B

Parameter	Value	Model	Full-wave sim.
$L_{1b}$ , mm	7.95	n/a	n/a
$W_{1b}$ , mm	2.75	n/a	n/a
$L_{2b}$ , mm	11.2	n/a	n/a
$W_{2b}$ , mm	0.2	n/a	n/a
$d_{1b}$ , mm	2.45	n/a	n/a
$f_{ob}$ , GHz	n/a	0.99	0.984
$f_{sb}$ , GHz	n/a	7.42	7.109

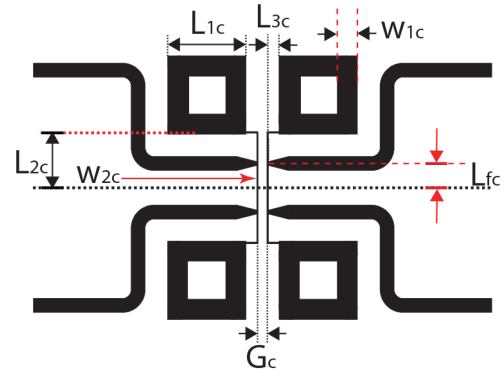


**Fig. 13** Most extended CM noise suppression prototype filter  $R_z = 0.3$  and  $N = 0.3$ .  $G_c = 1.027$  mm,  $L_{fc} = 3.046$  mm

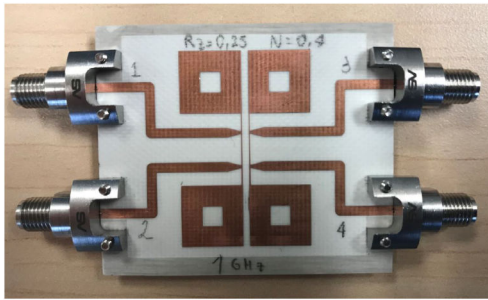
**Table 3** Dimensions and resonant frequencies of resonator C

Parameter	Value	Model	Full-wave sim.
$L_{1c}$ , mm	9.9	n/a	n/a
$W_{1c}$ , mm	2.6	n/a	n/a
$L_{2c}$ , mm	6.94	n/a	n/a
$W_{2c}$ , mm	0.25	n/a	n/a
$L_{3c}$ , mm	1.44	n/a	n/a
$d_{1c}$ , mm	4.7	n/a	n/a
$f_{oc}$ , GHz	n/a	0.99	0.942
$f_{sc}$ , GHz	n/a	5.99	6.37
$f_{occ}$ , GHz	n/a	5.04	4.75

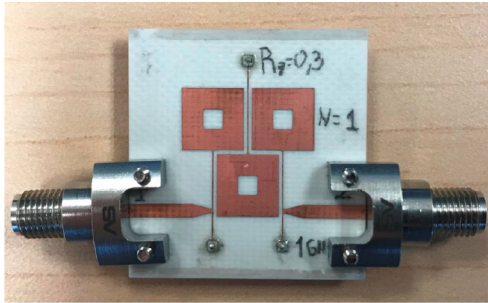
## 6 Conclusions

A method to design single-ended or balanced filters with extended DM stopband, extended CM noise suppression with a compact size has been proposed. This method uses a numerical method to solve the general resonance condition of a closed-loop resonator with either a short or open stub based on the ideal transmission lines model. The resonator's properties were analysed to obtain the best combination of parameters  $R_z$  and  $N$  that provides the optimal cases for the spurious frequency, CM resonant frequency and size. Size and spurious frequency can be improved by choosing a small value for the impedance ratio ( $R_z$ ) and a length ratio ( $N$ ) equal to 1. The CM resonant frequency can be improved by choosing a small value for the impedance ratio and a length ratio equal to 0.5.

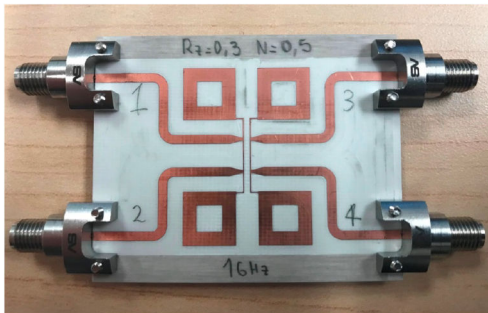
The theoretical analysis was used to design three filters to operate at 1 GHz with compact size, and either an extended DM stopband and extended CM noise suppression. The size of the smallest filter was  $0.093\lambda_g \times 0.122\lambda_g$ . The optimal out-band rejection is better than 30 dB up to  $8.2f_c$  and the optimal CM rejection was better than 20 dB up to  $6.64f_c$ .



a



b



c

**Fig. 14** Fabricated filters  
(a) Filter A, (b) Filter B, (c) Filter C

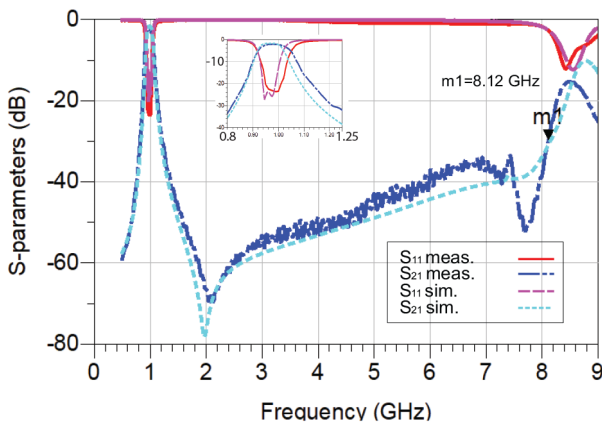
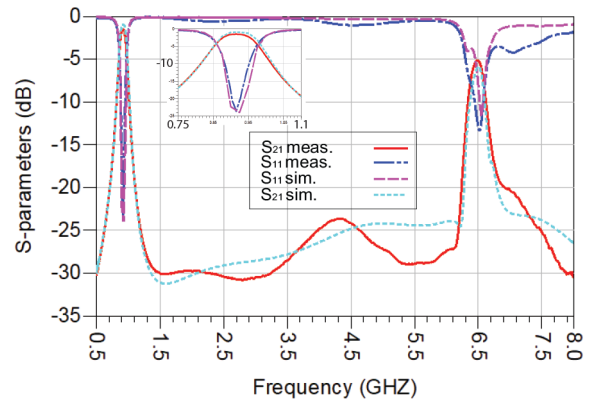


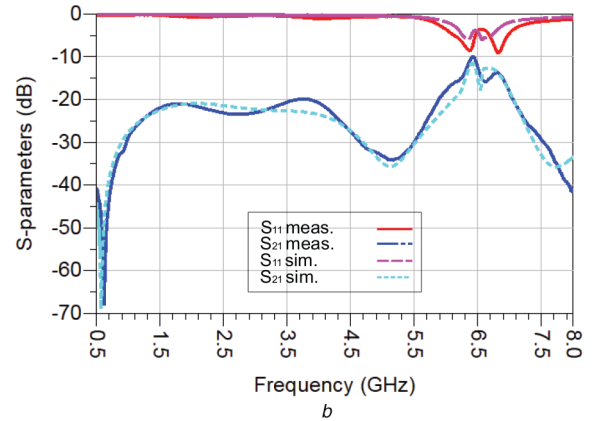
**Fig. 15** Filter B response

## 7 Acknowledgments

This research was supported by the Natural Sciences and Engineering Research Council (NSERC) R6PIN-2016-04784. The authors thank Matt Brown for insightful discussions.

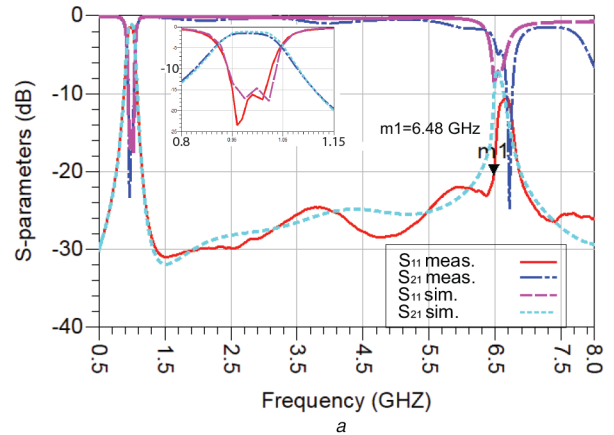


a

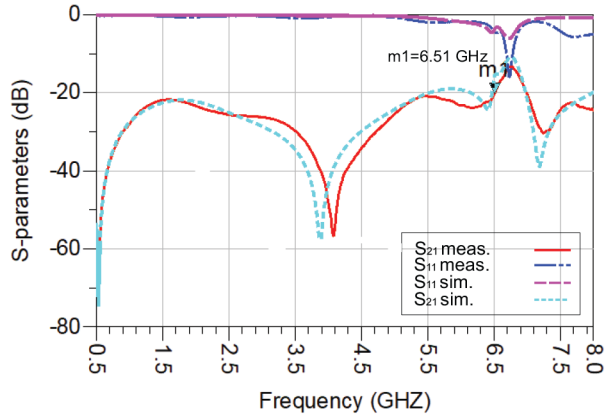


b

**Fig. 16** Filter A responses  
(a) DM, (b) CM



a



b

**Fig. 17** Filter C responses  
(a) DM, (b) CM

**Table 4** Comparison table between differential filters **A** and **C** and related works

Ref.	$f_c$ , GHz	FBW	Order	Insertion loss at $f_o$ , dB	DM stopband up to	CM stopband up to	Size ( $\lambda_g^2$ )
[4]	1.02	12	4	3.51	$5.65f_c, <-30$ dB	$3.43f_c, <-30$ dB	0.0473
[10]	2.39	2.5	2	<2	$2.72f_c, <-33$ dB	$2.72f_c, <-20$ dB	0.043
[11]	1.02	9.83	4	1.767	$5.63f_c, <-40$ dB	$3.7f_c, <-40$ dB	0.034
[12]	1.8	55.4	5	<1	$5.7f_c, <-30$ dB	$3.6f_c, <-22$ dB	0.245
This Filter <b>A</b>	0.917	13	2	1.5	$6.8f_c, <-20$ dB	$6.42f_c, <-20$ dB	0.025
This Filter <b>C</b>	0.98	12.8	2	1.52	$6.61f_c, <-20$ dB	$6.64f_c, <-20$ dB	0.024

**Table 5** Comparison table between single-ended Filter **B** and related works

Ref.	$f_c$ , GHz	FBW	Order	Insertion loss at $f_o$ , dB	Stopband up to	Size ( $\lambda_g^2$ )
[5]	1.95	14.72	3	3.3	$4f_c, <-20$ dB	0.017
[6]	2.39	3.8	3	3	$12f_c, <-40$ dB	0.01
[14]	2.45	45	3	1.3	$5.7f_c, <-27$ dB	0.021
[16]	3.535	15.6	4	1.6	$3f_c, <-34$ dB	0.042
This Filter <b>B</b>	0.99	13	3	2.09	$8.2f_c, <-30$ dB	0.011

## 8 References

- [1] Wu, C., Wang, C., Chen, C.H.: 'Novel balanced coupled-line bandpass filters with common-mode noise suppression', *IEEE Trans. Microw. Theory Techn.*, 2007, **55**, (2), pp. 287–295
- [2] Shiue, G.H., Shiu, J.H., Chiu, P.W.: 'Analysis and design of crosstalk noise reduction for coupled striplines inserted guard trace with an open-stub on time-domain in high-speed digital circuits', *IEEE Trans. Compon., Packag. Manuf. Technol.*, 2011, **1**, (10), pp. 1573–1582
- [3] Arbelaez-Nieto, A., Cruz-Perez, E., Olvera-Cervantes, J.L., et al.: 'The perfect balance-a design procedure for balanced bandpass filters [application notes]', *IEEE Microw. Mag.*, 2015, **16**, (10), pp. 54–65
- [4] Wu, C., Wang, C., Chen, C.H.: 'Stopband-extended balanced bandpass filter using coupled stepped-impedance resonators', *IEEE Microw. Wirel. Compon. Lett.*, 2007, **17**, (7), pp. 507–509
- [5] Escobar-Pelaez, J.A., Olvera-Cervantes, J.L., Corona-Chavez, A., et al.: 'A bandpass filter with compact size and extended stopband using closed-loop transmission-lines and short-circuited stubs', *Prog. Electromagn. Res.*, 2012, **35**, pp. 83–88
- [6] Chu, P., Guo, L., Zhang, L., et al.: 'Wide stopband bandpass filter implemented by stepped impedance resonator and multiple in-resonator open stubs', *IEEE Access*, 2019, **7**, pp. 140631–140636
- [7] Ouyang, Z., Wang, D., Chu, Q.: 'Compact balanced filters with enhanced differential-mode out-of-band response using coupled slotline structure'. *IEEE MTT-S Int. Wireless Symp.*, Chengdu, China, 2018, pp. 1–3
- [8] Xiang, K., Chen, F.: 'Compact microstrip bandpass filter with multispurious suppression using quarter-wavelength and half-wavelength uniform impedance resonators', *IEEE Access*, 2018, **6**, pp. 20364–20370
- [9] Gomez-Garcia, R., Loeches-Sanchez, R., Psychogiou, D., et al.: 'Dual-passband filters and extended-stopband wide-band bandpass filters based on generalized stub-loaded planar circuits'. *IEEE Int. Microwave Symp.*, Honolulu, HI, USA, 2017, pp. 368–371
- [10] Gu, H., Ge, L., Xu, L.: 'Simple dual-mode balanced bandpass filter with high selectivity and extended common-mode noise suppression', *Electron. Lett.*, 2018, **54**, (13), pp. 833–835
- [11] Olvera-Cervantes, J.L., Corona-Chavez, A.: 'Microstrip balanced bandpass filter with compact size, extended-stopband and common-mode noise suppression', *IEEE Microw. Wirel. Compon. Lett.*, 2013, **23**, (10), pp. 530–532
- [12] Sans, M., Selga, J., Velez, P., et al.: 'Compact wideband balanced bandpass filters with very broad common-mode and differential-mode stopbands', *IEEE Trans. Microw. Theory Techn.*, 2018, **66**, (2), pp. 737–750
- [13] Corona-Chavez, A., Olvera-Cervantes, J.L., Saavedra, C.E.: 'Balanced filter with parallel resonances for very wide band common mode rejection', *J. Electromagn. Waves Appl.*, 2015, **29**, (8), pp. 1060–1067
- [14] Huang, P., Hsieh, T., Tang, C.: 'A design of the compact microstrip bandpass filter with a wide passband and broad stopband'. *IEEE Int. Microwave Symp.*, San Francisco, CA, USA, 2016, pp. 1–4
- [15] Tantivivat, S., Razalli, M.S., Ibrahim, S.Z.: 'Miniature microstrip bandpass filters based on quadruple-mode resonators with less via'. *IEEE MTT-S Int. Conf. on Microwaves for Intelligent Mobility*, 2017, pp. 1–4
- [16] Rao, X., Huang, T., Huang, Y.M., et al.: 'Size-miniaturized bandpass filter made of folded stepped-impedance resonators with adjacent and nonadjacent coupling for selectivity enhancement'. *Progress in Electromagnetics Research Symp.*, Singapore, 2017, pp. 3045–3048
- [17] Qiu, L., Chu, Q.: 'Balanced bandpass filter using stub-loaded ring resonator and loaded coupled feed-line', *IEEE Microw. Wirel. Compon. Lett.*, 2015, **25**, (10), pp. 654–656
- [18] Kim, C.H., Chang, K.: 'Wideband ring resonator bandpass filter with dual stepped impedance stubs'. *IEEE Int. Microwave Symp.*, Anaheim, CA, USA, 2010, pp. 229–232
- [19] Jankovic, N., Radonic, V., Crnojevi-Bengin, V., et al.: 'A compact dual-band bandpass filter using folded quarter-wavelength resonators'. *European Microwave Conf.*, Amsterdam, Netherlands, 2012, pp. 360–363